Electronic Supplementary Material (ESI) for Journal of Materials Chemistry C.
This journal is © The Royal Society of Chemistry 2023

Electronic Supplementary Information

for

A nonbenzenoid acepleiadylene derivative with small band gap for near-infrared organic phototransistors

Pengcai Liu,[†,a] Lin Fu,[†,a] Xiao-Yu Tang,[a] Rui Xue,[a] Lijuan Zhang,[a] Jiawen Cao,[a] and Xiao-Ye Wang*[,a]

[a]State Key Laboratory of Elemento-Organic Chemistry, Frontiers Science Center for New Organic Matter, College of Chemistry, Nankai University, Weijin Road 94, Tianjin 300071, China

*Email: xiaoye.wang@nankai.edu.cn

[†]These authors contributed equally.

Table of Contents

1. General Methods

All commercial reagents and solvents were used as received without further purification unless otherwise mentioned. Anhydrous toluene, tetrahydrofuran, CH_2Cl_2 were obtained from an Ultinate Solvent System 4S (USS-4S). Column chromatography was performed with silica gel (particle size 0.063-0.200 mm) and thin layer chromatography (TLC) was performed on silica gel with GF254 indicator. All yields given refer to isolated yields unless otherwise noted. Nuclear magnetic resonance (NMR) spectra were recorded on an AVANCE 400 MHz Bruker spectrometer. Chemical shifts were reported in ppm. Coupling constants (*J* values) were reported in Hertz. ^{1}H NMR chemical shifts were referenced to $CHCl_3$ (7.260 ppm) and DMSO-d_5 (2.500 ppm). ^{13}C NMR chemical shifts were referenced to $CDCl_3$ (77.00 ppm) and DMSO-d_6 (39.52 ppm). The following abbreviations were used for multiplicities: s = singlet, d = doublet, t = triplet, m = multiplet. High-resolution mass spectrometry (HRMS) was performed on a Solarix scimax MRMS by matrix-assisted laser desorption/ionization (MALDI). Absorption spectra were recorded on an Analytikjena Specord 210 Plus UV-Vis spectrophotometer. Photoluminescence spectra were recorded on an Edinburgh FS5 Spectrofluorometer. The electrochemical measurements were carried out in anhydrous THF containing 0.1 M n-Bu_4NPF_6 as supporting electrolyte (scan rate: 100 mV s^{-1}.) under argon atmosphere on a CHI 620E electrochemical analyzer. A three-electrode system with glassy carbon as working electrode, Ag/AgCl as reference electrode, platinum wire as counter electrode was applied. The potential was calibrated against ferrocene/ferrocenium couple. Thermal gravity analyses (TGA) were carried out on a NETZSCH METTLER-TOLEDO TG209 METTLER3+ analyzer. Thin-film X-ray diffraction (XRD) was carried out on a SmartLab9KW X-ray diffractometer at a voltage of 45 kV and a current of 200 mA with the reflection mode using Cu K_α radiation (λ = 1.542 Å). Tapping-mode atomic force microscope (AFM) images were recorded using a Bruker Dimensional Icon AFM in air.

2. Synthetic Procedure

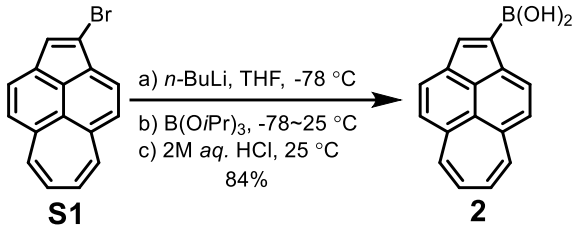

cyclohepta[*fg*]acenaphthylen-1-ylboronic acid (2). To a Schlenk flask charged with **S1**[1] (579 mg, 2.06 mmol) was added THF (42 mL) under argon. After the solution was cooled to –78 °C, *n*-BuLi (1.5 mL, 2.4 M in hexane) was added and the mixture was stirred for 1 h before B(O*i*Pr)$_3$ (775 mg, 4.12 mmol) was added dropwise at that temperature. The reaction was allowed to warm up to room temperature and was stirred for another 8 h. After hydrochloric acid (30 mL, 2.0 M) was added, the reaction mixture was stirred for another 2 h and then extracted with ethyl acetate for three times. The combined organic layer was washed with water and brine, and dried over $MgSO_4$. After removal of the solvent under reduced pressure, the residue was purified by flash column chromatography over silica gel (eluent: MeOH/CH_2Cl_2 = 1 : 5) to afford 425 mg (yield: 84%) of **2** as a red solid. ^{1}H NMR (400 MHz, DMSO-d_6, 298 K, ppm) δ 8.77 (d, J = 7.4 Hz, 1H), 8.50 – 8.43 (m, 2H), 8.30 (s, 2H), 8.11 – 8.04 (m, 2H), 7.92 – 7.83 (m, 2H), 7.05 – 6.92 (m, 2H).^{13}C NMR (101 MHz, DMSO-d_6, 298 K, ppm) δ 138.21, 138.10, 137.17, 136.84, 136.47, 135.46, 134.42, 127.68, 127.64, 127.53, 127.36, 127.33, 126.83, 126.54, 126.52.

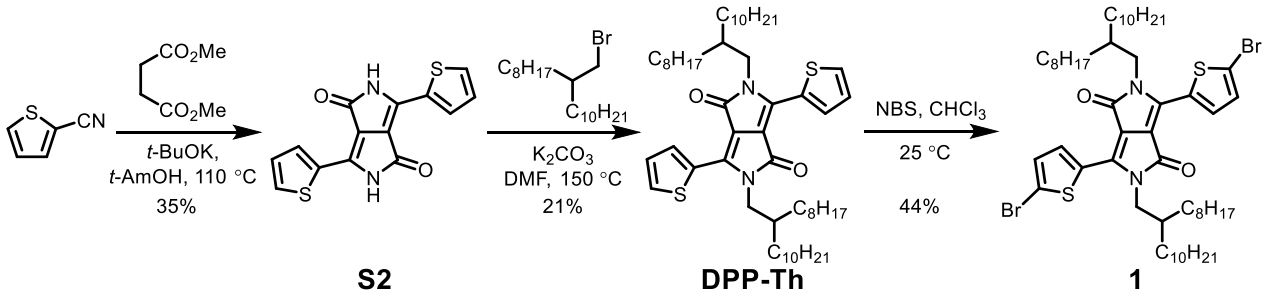

Compound **1** was synthesized following the literature.[2]

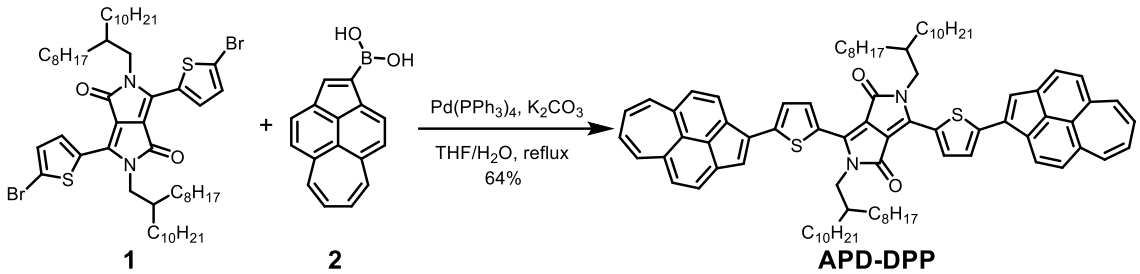

3,6-bis(5-(cyclohepta[*fg*]acenaphthylen-1-yl)thiophen-2-yl)-2,5-bis(2-octyldodecyl)-2,5-dihydropyrrolo[3,4-*c*]pyrrole-1,4-dione (APD-DPP). To a Schlenk flask charged with **1** (163 mg, 0.160 mmol), **2** (123 mg, 0.500 mmol), $Pd(PPh_3)_4$ (23 mg, 0.020 mmol), and K_2CO_3 (70 mg, 0.50 mmol) was added THF and H_2O (9 mL + 1 mL) under argon. Then the mixture was heated to reflux for 24 h. After cooled to room temperature and quenched by water, the mixture was extracted with CH_2Cl_2 for three times. The combined organic layer was washed with water and brine and dried over $MgSO_4$. After removal of the solvent under reduced pressure, the residue was purified by column chromatography over silica gel (eluent: hexane/CH_2Cl_2 = 2 : 1) and further recrystallization from CH_2Cl_2/MeOH to afford 129 mg (yield: 64%) of APD-DPP as a black solid. ^{1}H NMR (400 MHz, $CDCl_3$, 298 K, ppm) δ 9.22 (d, J = 4.2 Hz, 2H), 8.66 (d, J = 7.5 Hz, 2H), 8.29 (d, J = 7.5 Hz, 2H), 8.05 (s, 2H), 7.93 (dd, J = 16.9, 7.6 Hz, 4H), 7.79 (d, J = 4.3 Hz, 2H), 7.74 (d, J = 10.8 Hz, 4H), 7.02 – 6.88 (m, 4H), 4.13 (d, J = 7.7 Hz, 4H), 2.17 – 2.03 (m, 2H), 1.47 – 1.40 (m, 12H), 1.31 – 1.17 (m, 52H), 0.88 – 0.80 (m, 12H). ^{13}C NMR (101 MHz, CS_2/$CDCl_3$, 298 K, ppm) δ 161.01, 145.31, 138.91, 138.44, 138.33, 137.31, 137.21, 136.77, 133.36, 131.16, 130.98, 129.00, 127.94, 127.77, 127.43, 127.34, 127.22, 127.12, 126.07, 125.84, 125.61, 122.74, 108.20, 46.08, 38.20, 32.00, 31.32, 30.37, 29.87, 29.80, 29.51, 29.49, 26.51, 22.86, 14.20. HRMS (MALDI) *m*/*z*: Calcd. for $C_{86}H_{104}N_2O_2S_2$, 1261.7539; Found, 1261.7597 $[M]^+$.

1Py-DPP and 2Py-DPP were synthesized according to the literature based on a modified procedure.[3] The characterization data are consistent with those in the literature.

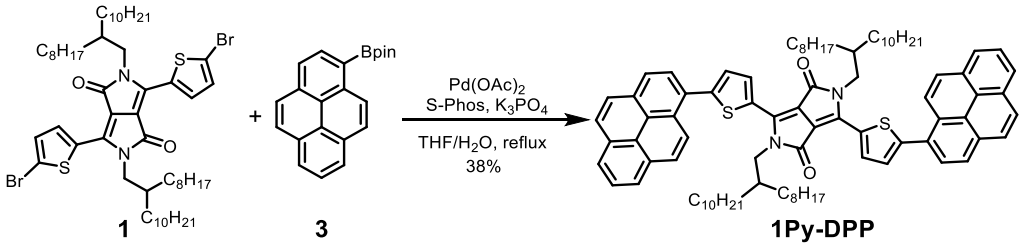

2,5-bis(2-octyldodecyl)-3,6-bis(5-(pyren-1-yl)thiophen-2-yl)-2,5-dihydropyrrolo[3,4-c]pyrrole-1,4-dione (1Py-DPP). To a Schlenk flask charged with **1** (153 mg, 0.150 mmol), **3** (148 mg, 0.451 mmol), $Pd(OAc)_2$ (4.5 mg, 0.020 mmol), S-Phos (16 mg, 0.040 mmol), and K_3PO_4 (96 mg, 0.45 mmol) was added THF and H_2O (9 mL + 1 mL) under argon. Then the mixture was heated to reflux for 24 h. After cooled to room temperature and quenched by water, the mixture was extracted with CH_2Cl_2 for three times. The combined organic layer was washed with water and brine and dried over $MgSO_4$. After removal of the solvent under reduced pressure, the residue was purified by column chromatography over silica gel (eluent: hexane/CH_2Cl_2 = 2 : 1) and further recrystallization from CH_2Cl_2/MeOH to afford 72 mg (yield: 38%) of 1Py-DPP as a deep blue solid. ^{1}H NMR (400 MHz, $CDCl_3$, 298 K, ppm) δ 9.20 (d, J = 3.9 Hz, 2H), 8.57 (d, J = 9.3 Hz, 2H), 8.25 – 8.20 (m, 6H), 8.17 – 8.03 (m, 10H), 7.60 (d, J = 4.0 Hz, 2H), 4.15 (d, J = 7.7 Hz, 4H), 2.17 – 2.07 (m, 2H), 1.46 – 1.15 (m, 64H), 0.87 – 0.80 (m, 12H). ^{13}C NMR (101 MHz, CS_2/$CDCl_3$, 298 K, ppm) δ 161.59, 148.34, 139.89, 136.39, 131.57, 131.34, 130.79, 130.35, 129.30, 128.89, 128.53, 128.30, 128.10, 127.23, 126.32, 125.71, 125.37, 125.05, 124.67, 124.60, 124.40, 108.11, 46.33, 38.09, 31.93, 31.92, 31.31, 30.20, 29.73, 29.69, 29.64, 29.39, 26.40, 22.74, 22.72, 14.13.

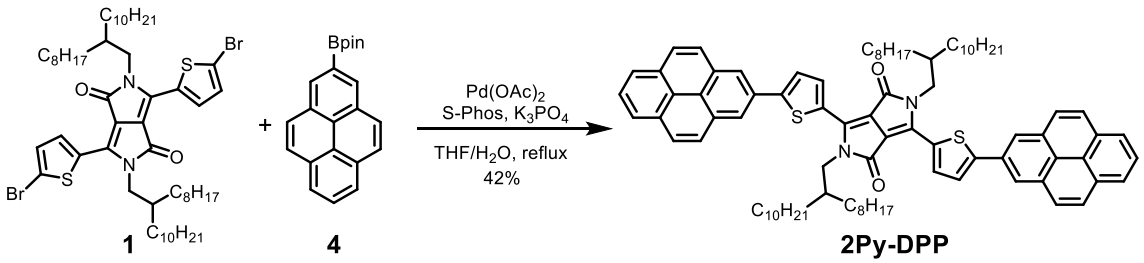

2,5-bis(2-octyldodecyl)-3,6-bis(5-(pyren-2-yl)thiophen-2-yl)-2,5-dihydropyrrolo[3,4-c]pyrrole-1,4-dione (2Py-DPP). To a Schlenk flask charged with **1** (153 mg, 0.150 mmol), **4** (148 mg, 0.451 mmol), $Pd(OAc)_2$ (4.5 mg, 0.020 mmol), S-Phos (16 mg, 0.040 mmol), and K_3PO_4 (96 mg, 0.45 mmol) was added THF and H_2O (9 mL + 1 mL) under argon. Then the mixture was heated to reflux for 24 h.

After cooled to room temperature and quenched by water, the mixture was extracted with CH_2Cl_2 for three times. The combined organic layer was washed with water and brine and dried over $MgSO_4$. After removal of the solvent under reduced pressure, the residue was purified by column chromatography over silica gel (eluent: hexane/CH_2Cl_2 = 2 : 1) and further recrystallization from CH_2Cl_2/MeOH to afford 80 mg (yield: 42%) of 2Py-DPP as a deep blue solid. ^{1}H NMR (400 MHz, $CDCl_3$, 298 K, ppm) δ 9.09 (d, J = 4.0 Hz, 2H), 8.30 (s, 4H), 8.10 (d, J = 7.5 Hz, 4H), 8.05 – 7.96 (m, 8H), 7.93 (t, J = 7.6 Hz, 2H), 7.67 (d, J = 3.8 Hz, 2H), 4.10 (d, J = 7.7 Hz, 4H), 2.10 – 1.98 (m, 2H), 1.50 – 1.16 (m, 64H), 0.87 – 0.80 (m, 12H). ^{13}C NMR (101 MHz, CS_2/$CDCl_3$, 298 K, ppm) δ 160.78, 149.34, 138.94, 137.04, 131.24, 130.75, 130.22, 129.09, 127.97, 126.91, 125.98, 125.20, 124.53, 124.21, 124.06, 121.59, 107.89, 45.89, 38.06, 31.97, 31.36, 30.36, 29.92, 29.86, 29.80, 29.77, 29.51, 29.47, 26.58, 22.85, 14.19.

3. TGA Curves of APD-DPP, 1Py-DPP, and 2Py-DPP

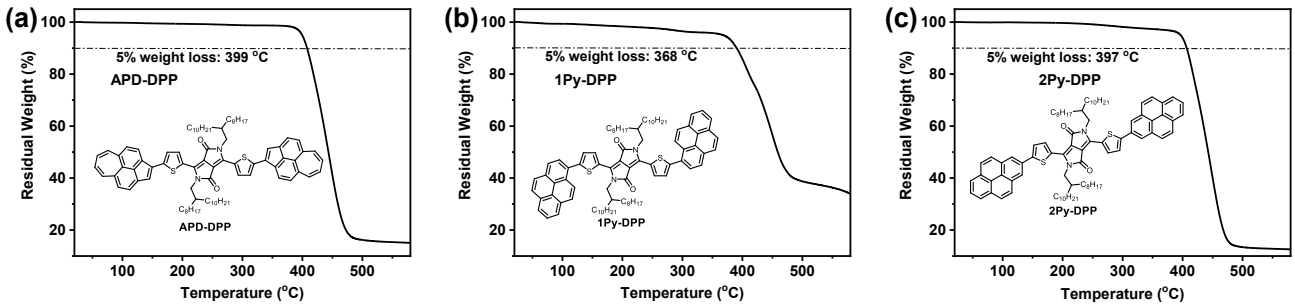

Figure S1. TGA curves of (a) APD-DPP (5% loss: 399 °C); (b) 1Py-DPP (5% loss: 368 °C); and (c) 2Py-DPP (5% loss: 397 °C).

4. Photophysical and Electrochemical Properties

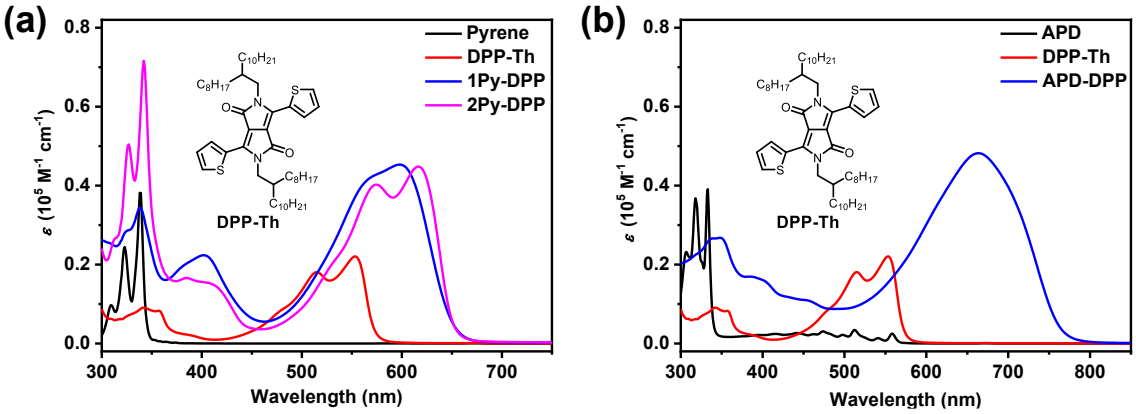

Figure S2. UV-Vis absorption spectra of (a) pyrene, DPP-Th, 1Py-DPP, and 2Py-DPP; (b) APD, DPP-Th, and APD-DPP in 1×10^{-5} M toluene solutions.

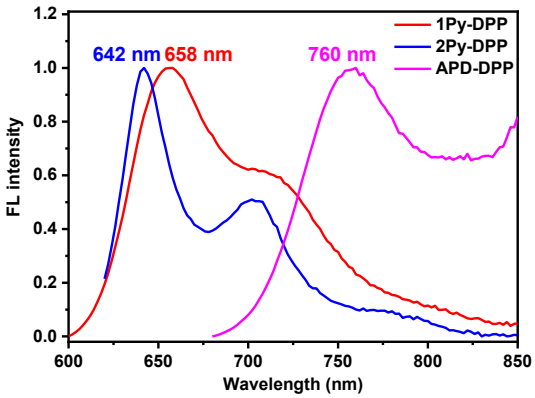

Figure S3. Fluorescence spectra of 1Py-DPP (excitation wavelength: 580 nm), 2Py-DPP (excitation wavelength: 610 nm), and APD-DPP (excitation wavelength: 650 nm) in 1×10^{-6} M toluene solutions.

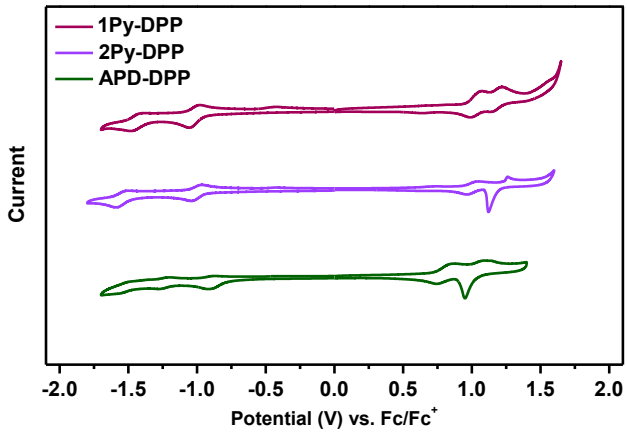

Figure S4. Cyclic voltammograms of APD-DPP, 1Py-DPP, and 2Py-DPP in THF with 0.1 M *n*-Bu_4NPF_6 as supporting electrolyte and ferrocene as an external standard.

Table S1. Summary of the photophysical and electrochemical properties.[a]

Compd.	λ (nm) Solution	λ (nm) Film	λ_{onset} (nm)	E_g^{opt} (eV)	$LUMO^{CV}$ (eV)	$HOMO^{CV}$ (eV)	E_g^{CV} (eV)
APD-DPP	664/384/347	765/692	780	1.59	–4.02	–5.53	1.51
1Py-DPP	598/402/338	672/613	667	1.86	–3.85	–5.76	1.91
2Py-DPP	617/385/342	654/595	667	1.86	–3.86	–5.74	1.88

[a]Definitions: E_g^{opt} is the optical energy gap calculated according to the equation $E_g^{opt} = 1240/\lambda_{onset}$; λ_{onset} is taken from the spectra in toluene solutions. The $HOMO^{CV}$ and $LUMO^{CV}$ energy levels are calculated according to the equations HOMO = −(4.80 + E_{ox}^{onset}) and LUMO = −(4.80 + E_{red}^{onset}), where E_{ox}^{onset} and E_{red}^{onset} are the onset potentials of the first oxidative and reductive waves, respectively. E_g^{CV} is calculated according to the equation $E_g^{CV} = LUMO^{CV} - HOMO^{CV}$.

5. Device Fabrication and Characterizations

For thin-film transistors, top-contact/bottom-gate (TC/BG) device configuration was adopted. After ultrasonicated in acetone, cleaning reagent, deionized water and isopropanol, n^{++}-Si wafers with 300 nm thermally grown silicon dioxide (SiO_2/Si) were dried with nitrogen airflow and finally treated with oxygen plasma for 15 min. A solution of $Al(NO_3)_3$•$9H_2O$ in ethanol (0.1 M) was spin-coated onto the cleaned SiO_2/Si substrate at 5000 rpm for 40 s. The resulting film was baked at 300 °C for 30 min. To form the 12-cyclohexyldodecylphosphonic acid (CDPA) self-assembled monolayers (SAMs), the

$AlO_x/SiO_2/Si$ substrate was then immersed in a 0.3 mM solution of CDPA in isopropanol at room temperature for 12 h and then rinsed with isopropanol and dried with nitrogen airflow.[4] The organic semiconductor materials (APD-DPP, 1Py-DPP, and 2Py-DPP) were dissolved at the concentration of 2 mg mL^{-1} in trichloroethylene at 60 °C for 1 h. Then the solution was spin-coated on the CDPA-modified $AlO_x/SiO_2/Si$ substrates at 1500 rpm for 60 s. The samples were immediately placed on a hotplate for annealing. After annealing at specific temperatures for 30 min, Au (80 nm) was deposited under vacuum (4×10^{-4} Pa) via the shadow mask method as the top source and drain electrodes. The evaluations of the transistors were carried out on a probe stage using a Keysight B1500A as the parameter analyzer. The carrier mobility (μ) was calculated from the data in the saturated regime according to the equation $I_{SD} = (W/2L)\ \mu\ C_i\ (V_G\text{-}V_T)^2$, where I_{SD} is the source-drain current in the saturated regime. The average value and error bar (standard deviation) of carrier mobility at each condition were calculated from 30 devices. W and L are the semiconductor channel width and length, respectively (W = 1000 μm and L = 50 μm). C_i (10 nF cm^{-2} for CDPA-modified $AlO_x/SiO_2/Si$) is the capacitance per unit area of the gate dielectric layer. V_G and V_T are gate voltage and threshold voltage, respectively. V_T of the device was determined from the relationship between the square root of I_{SD} and V_G at the saturated regime. The OFET performance is shown in Figures S5 – S8 and Table S2.

The NIR detection performance of the original OFET devices is shown in Figure S9 and Table S3. For the optimization of the NIR OPT performance, an electron blocking layer MoO_3 was introduced into the original OFET devices. MoO_3 (10 nm) and Au (80 nm) were deposited sequentially under vacuum (4×10^{-4} Pa) via the shadow mask method as the electron blocking layer and source/drain electrodes, respectively. To demonstrate the NIR phototransistor application of APD-DPP, we chose the illumination light wavelength by considering the available light sources and the absorption intensity. We have NIR LEDs with adjustable illumination power in our laboratory with wavelengths of 730 nm, 810 nm, and 850 nm. According to the absorption spectrum of APD-DPP in the thin film, it shows significant absorption at 730 nm (around 70% absorbance of the maximum at 765 nm). Therefore, we chose the 730 nm LED light source to prove the NIR phototransistor application of APD-DPP. The light power density was measured by Thorlab PM100D with a Si photodetector. The NIR detection performance of the OPTs with MoO_3 layer is shown in Figure S10 and Table S4.

According to the transfer curves under the dark and light illumination (730 nm), three key parameters of OPTs were obtained based on the following formulas, including photosensitivity (P), photoresponsivity (R), and specific detectivity (D^*).

$$P = \frac{signal}{noise} = \frac{I_{\mathrm{ph}}}{I_{\mathrm{dark}}} = \frac{I_{\mathrm{light}} - I_{\mathrm{dark}}}{I_{\mathrm{dark}}}$$

$$R = \frac{I_{\mathrm{ph}}}{P_{\mathrm{opt}}} = \frac{I_{\mathrm{ph}}}{P_{\mathrm{int}}A}$$

$$D^* = \frac{RA^{1/2}}{(2qI_{\mathrm{dark}})^{1/2}}$$

I_{light} is the drain current under light irradiation; I_{dark} is the drain current under dark; A is the effective light illumination area of the semiconductor layer; P_{int} is the incident light power per unit area; q is the charge of an electron.

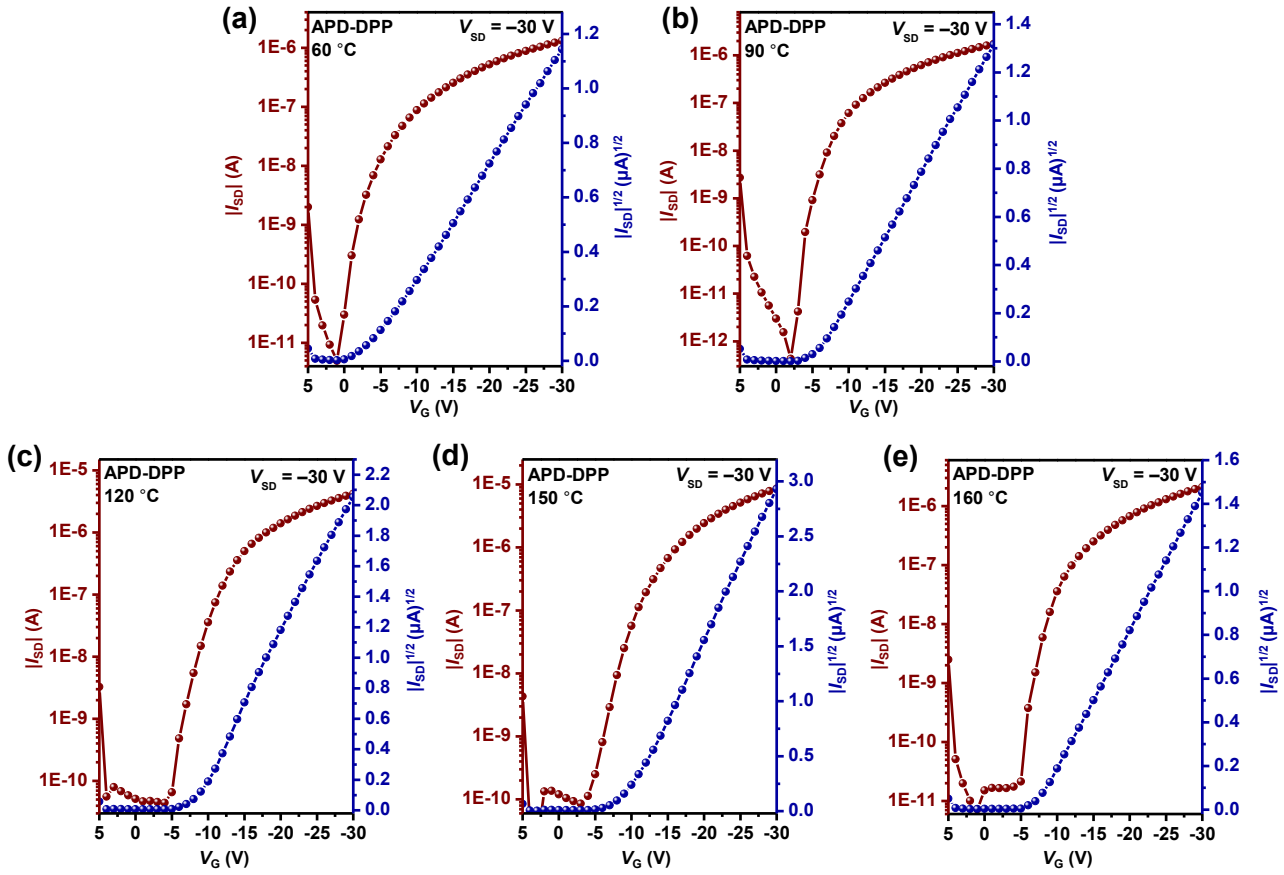

Figure S5. Transfer curves of APD-DPP at different annealing temperatures: (a) 60 °C; (b) 90 °C; (c) 120 °C; (d) 150 °C; (e) 160 °C.

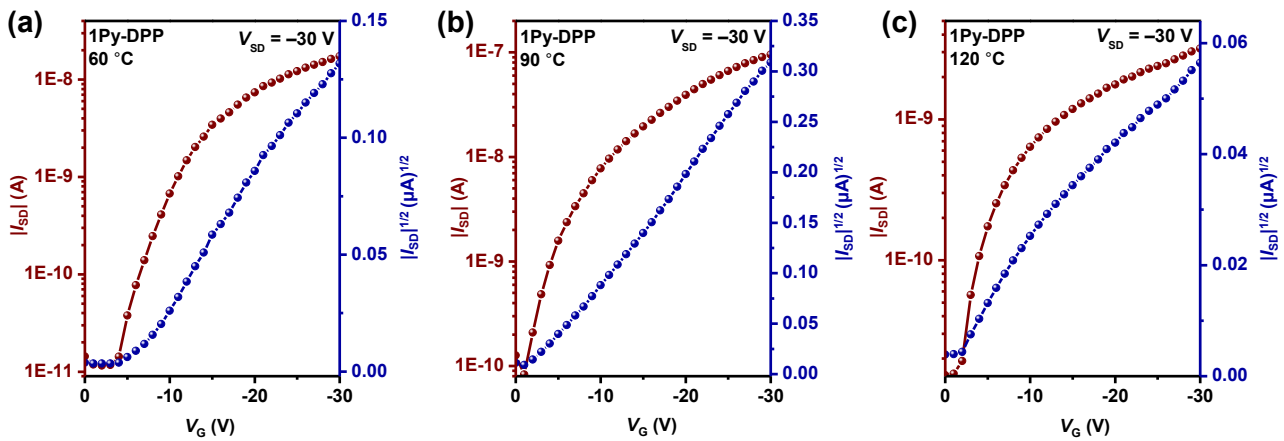

Figure S6. Transfer curves of 1Py-DPP at different annealing temperatures: (a) 60 °C; (b) 90 °C; (c) 120 °C.

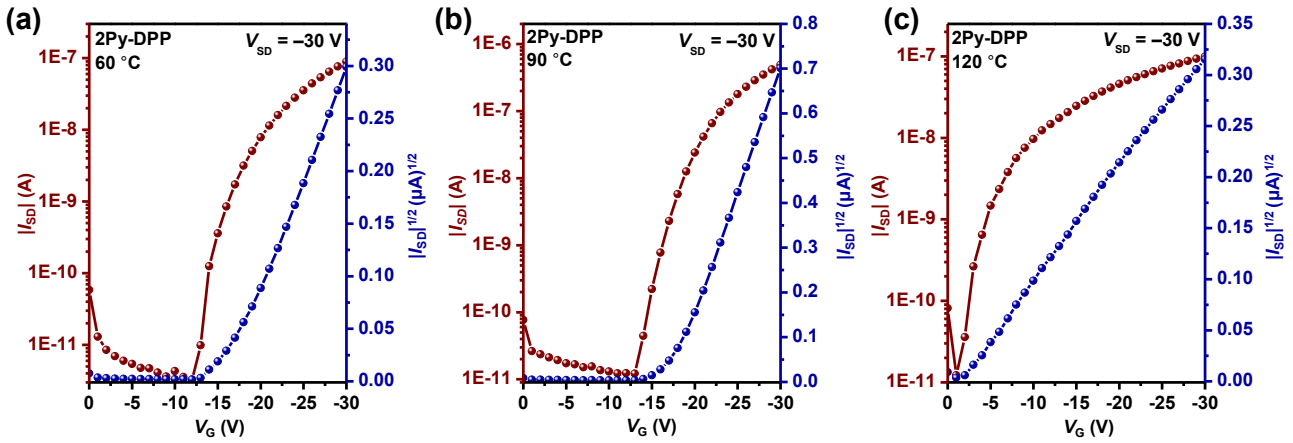

Figure S7. Transfer curves of 2Py-DPP at different annealing temperatures: (a) 60 °C; (b) 90 °C; (c) 120 °C.

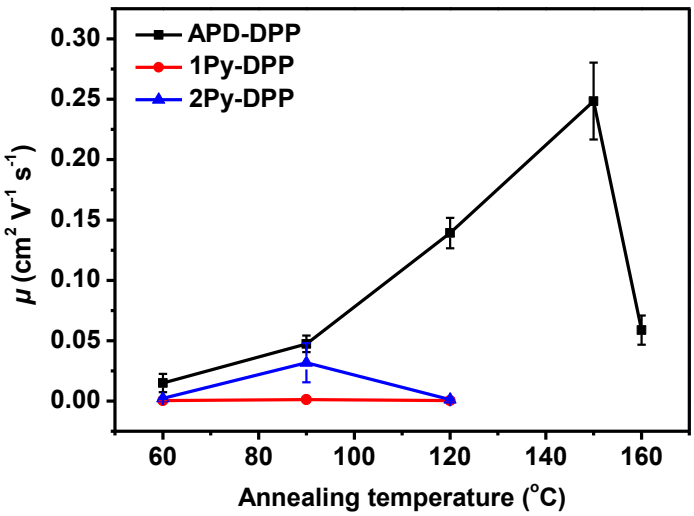

Figure S8. Average mobility as a function of the annealing temperature.

Table S2. Summary of the OFET performance of thin films annealed at different temperatures.

Compd.	T (°C)	μ_{max} ($cm^2\ V^{-1}\ s^{-1}$)	μ_{avg} ($cm^2\ V^{-1}\ s^{-1}$)	V_T (V)	I_{on}/I_{off}
APD-DPP	60	3.60×10^{-2}	0.015	–12.87	10^6
	90	5.80×10^{-2}	0.047	–9.90	10^6
	120	0.16	0.14	–11.45	10^6
	150	0.30	0.23	–8.86	10^6
	160	8.32×10^{-2}	0.059	–10.98	10^4
1Py-DPP	60	7.49×10^{-4}	3.44×10^{-4}	–8.21	10^3
	90	2.60×10^{-3}	1.20×10^{-3}	–7.74	10^3
	120	1.00×10^{-3}	4.64×10^{-4}	–11.23	10^3
2Py-DPP	60	9.25×10^{-3}	2.33×10^{-3}	–9.71	10^5
	90	6.38×10^{-2}	3.18×10^{-2}	–7.29	10^5
	120	2.33×10^{-3}	1.18×10^{-3}	–16.4	10^4

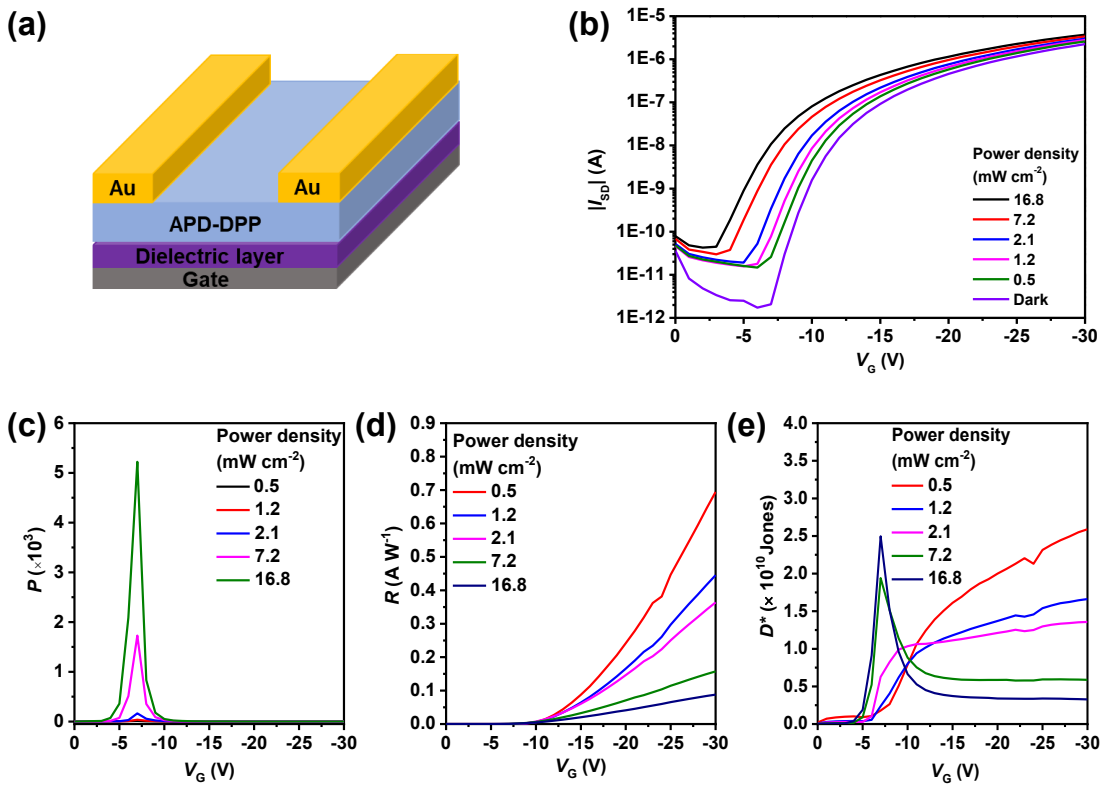

Figure S9. (a) Schematic illustration of the APD-DPP-based original OFET device. (b) Transfer characteristics of the original OFET device under NIR light with different power densities. (c-e) Gate-tunable behavior of NIR OPTs without MoO_3 layer under NIR light with different power densities: (c) photosensitivity (P); (d) photoresponsivity (R); (e) specific detectivity (D^*).

Table S3. NIR detection performance (the maximum of P, R, and D^*) of the original OFET devices under different power densities.

P_{int} (mW cm^{-2})	0.5	1.2	2.1	7.2	16.8
P	1.16×10^1	3.64×10^1	1.64×10^2	1.73×10^3	5.22×10^3
R (A W^{-1})	0.69	0.45	0.36	0.16	0.09
D^* (Jones)	2.59×10^{10}	1.66×10^{10}	1.36×10^{10}	1.94×10^{10}	2.50×10^{10}

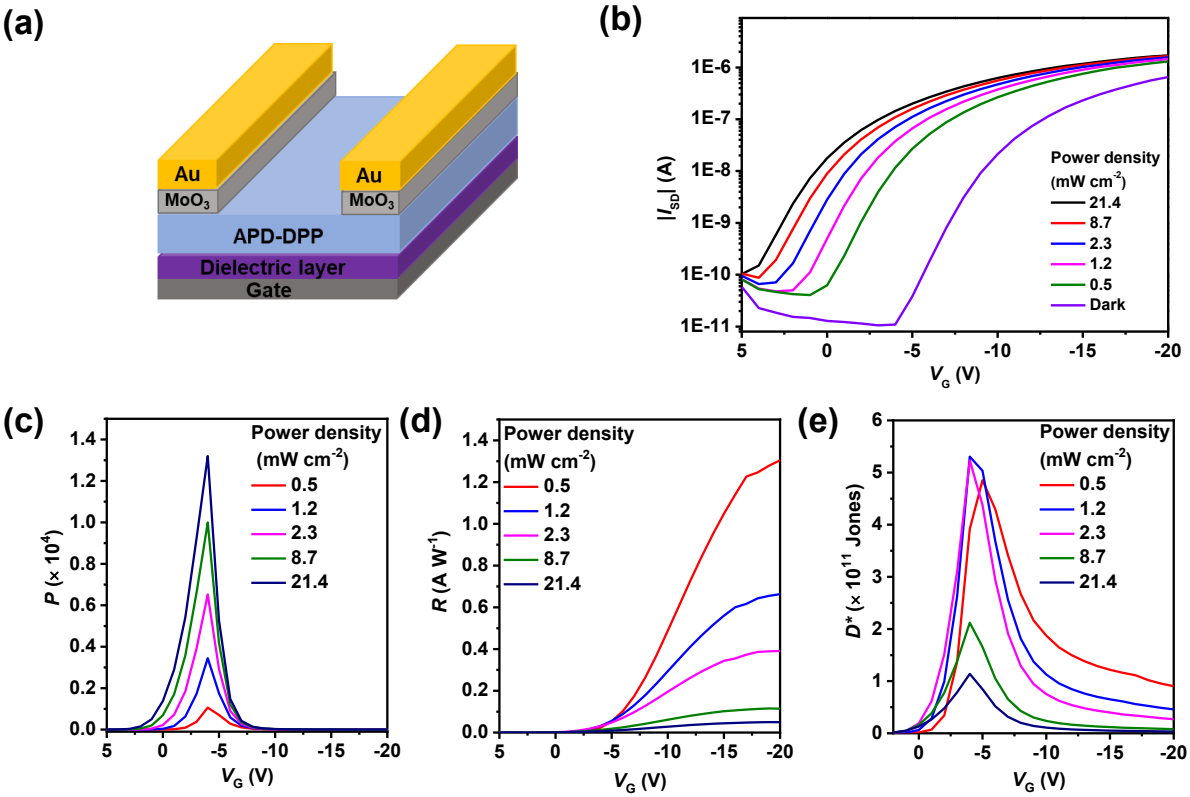

Figure S10. (a) Schematic illustration of the APD-DPP-based NIR OPTs with the MoO_3 layer. (b) Transfer characteristics of NIR OPTs with MoO_3 layer under NIR light with different power densities. (c-e) Gate-tunable behavior of NIR OPTs with MoO_3 layer under NIR light with different power densities: (c) photosensitivity (P); (d) photoresponsivity (R); (e) specific detectivity (D^*). Due to the introduction of MoO_3 layer, it is more conducive to hole injection, and the V_T shifts towards zero, so the V_G of the device with MoO_3 layer is set as 5 to −20 V during the measurement.

Table S4. NIR detection performance (the maximum of P, R, and D^*) of NIR OPTs with MoO_3 layer under different power densities.

P_{int} (mW cm^{-2})	0.5	1.2	2.3	8.7	21.4
P	1.06×10^3	3.45×10^3	6.52×10^3	1.00×10^4	1.32×10^4
R (A W^{-1})	1.30	0.66	0.39	0.11	0.05
D^* (Jones)	4.85×10^{11}	5.31×10^{11}	5.24×10^{11}	2.12×10^{11}	8.47×10^{10}

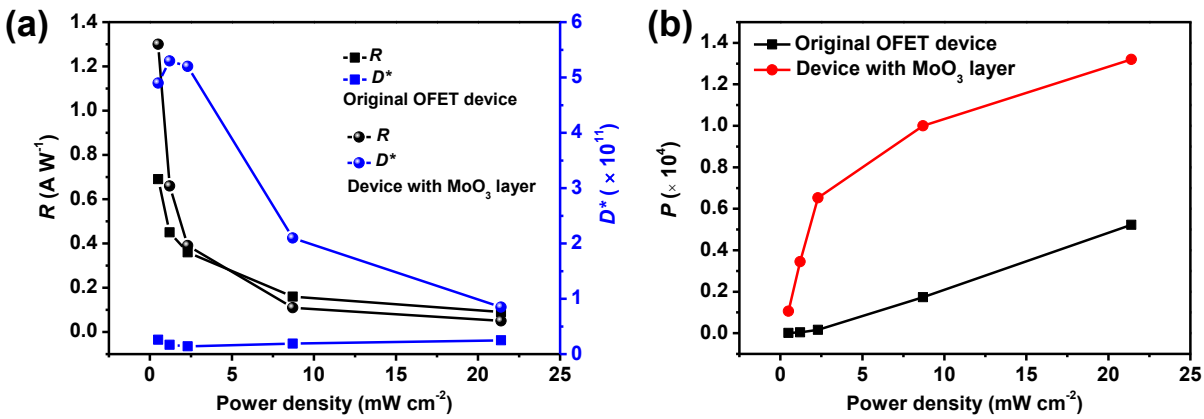

Figure S11. Comparison of NIR light detection performance between the original OFET device and the device with MoO_3 layer: (a) photoresponsivity (R) and specific detectivity (D^*); (b) photosensitivity (P). (Test parameters for the original OFET device: $V_{SD} = -30$ V, $V_G = -30$ V for R, $V_G = -7$ V for D^* and P. Test parameters for the device with MoO_3 layer: $V_{SD} = -20$ V, $V_G = -20$ V for R, $V_G = -4$ V for D^* and P).

Table S5. Comparison of the device performance of organic single-component NIR photodetectors.

Channel material	Mobility (cm^2 V^{-1} s^{-1}) Hole	Electron	Detection region (nm)	R (A W^{-1})	P	D^* (Jones)	Ref.
PPhTQ	0.09	0.06	1186	400	NA	NA	5
PBIBDF-TT	0.02	NA	808	0.44	3.3×10^4	NA	6
PIBDFBTO-HH	0.16	0.14	940	0.45	100	NA	7
pTTDPP-BT	0.066	0.115	450-850	NA	150	NA	8
BODIPY-BF2	NA	0.113	760/850/940	9450	1.04×10^4	NA	9
PIDTT-NDI	NA	4.7×10^{-4}	754	3.19	8.42×10^{-3}	NA	10
Y6	NA	0.032	850	0.27	870	5.6×10^{11}	11
DAP-based copolymers	0.4	NA	1060	560	1008	1.8×10^{12}	12

PODTPPD-BT	6×10^{-4}	NA	905	1.25×10^{-5}	6×10^{3}	NA	13
PDPP-8OBT	NA	9.44×10^{-5}	750	$<10^{-2}$	14	NA	14
PDPP-8OBT-NDI	0.041	0.023	810/905	0.001	4	NA	15
APD-DPP	**0.30**	**NA**	**730**	**1.30**	**1.34×10^{4}**	**5.31×10^{11}**	**This work**

6. Thin-Film Morphologies and Microstructures

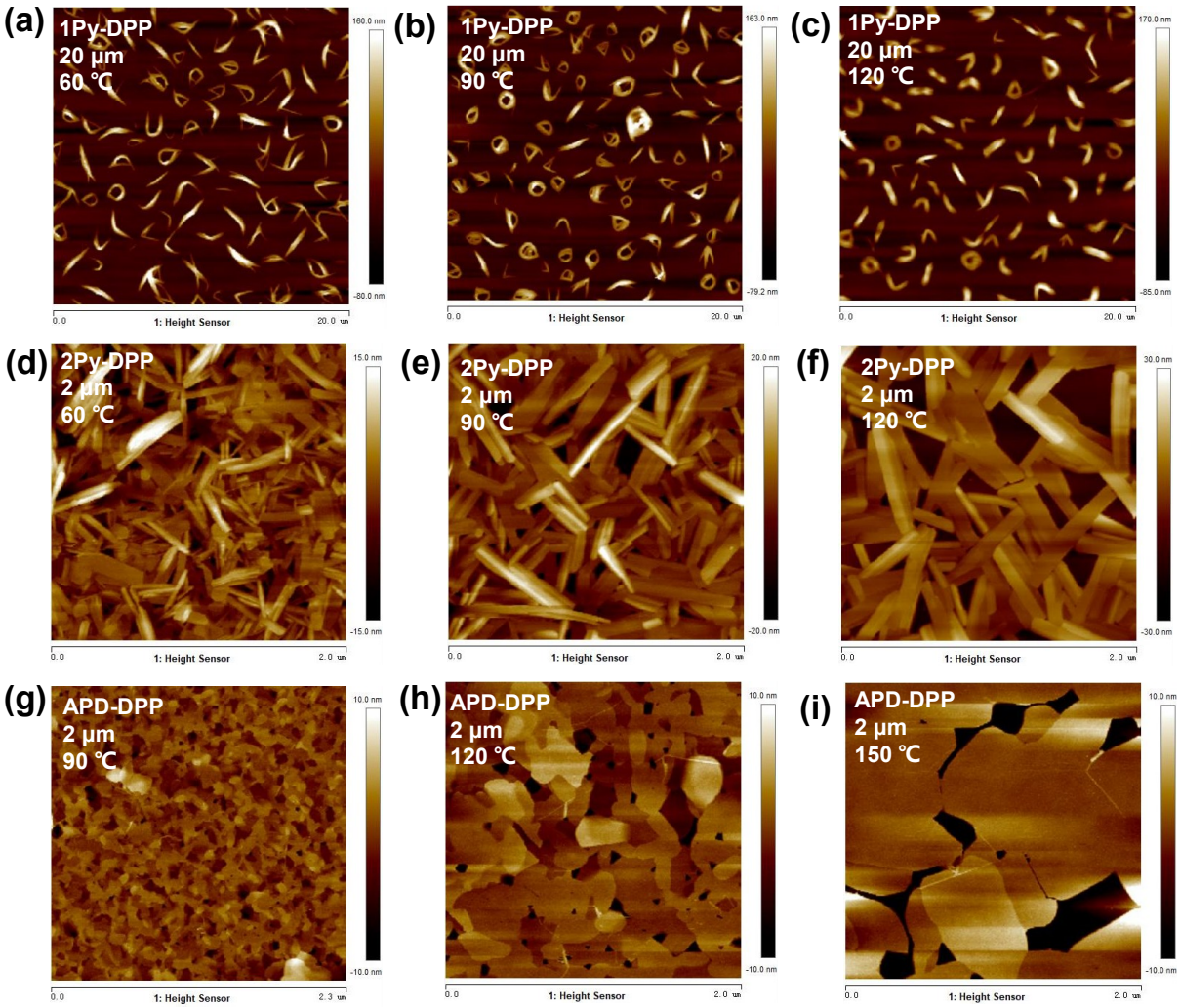

Figure S12. AFM height images of 1Py-DPP, 2Py-DPP, and APD-DPP films under different annealing temperatures: (a-c) 1Py-DPP film annealed at (a) 60 °C; (b) 90 °C; and (c) 120 °C; (d-f) 2Py-DPP film annealed at (d) 60 °C; (e) 90 °C; and (f) 120 °C; (g-i) APD-DPP film annealed at (g) 90 °C; (h) 120 °C; and (i) 150 °C.

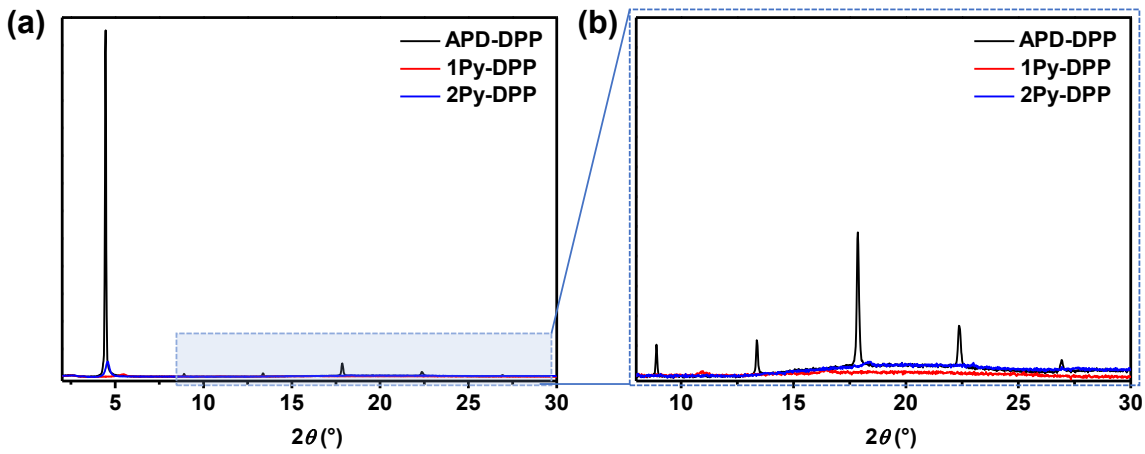

Figure S13. (a) XRD patterns of APD-DPP, 1Py-DPP, and 2Py-DPP thin films under the optimized condition (APD-DPP thin film annealed at 150 °C; 1Py-DPP and 2Py-DPP thin films annealed at 90 °C). (b) An enlarged view of the XRD patterns with the 2θ from 8° to 30°.

7. Theoretical Calculations

Theoretical calculations were performed using the Gaussian 09 software package.[16] All calculations were carried out using the density functional theory (DFT) method.[17] The geometries were optimized at the B3LYP/6-311G(d,p) level, and energies were calculated at the same level of theory. Time-dependent DFT (TD-DFT) calculations were performed at the B3LYP/6-311G(d,p) level. Alkyl chains were replaced by methyl groups for computational simplicity.

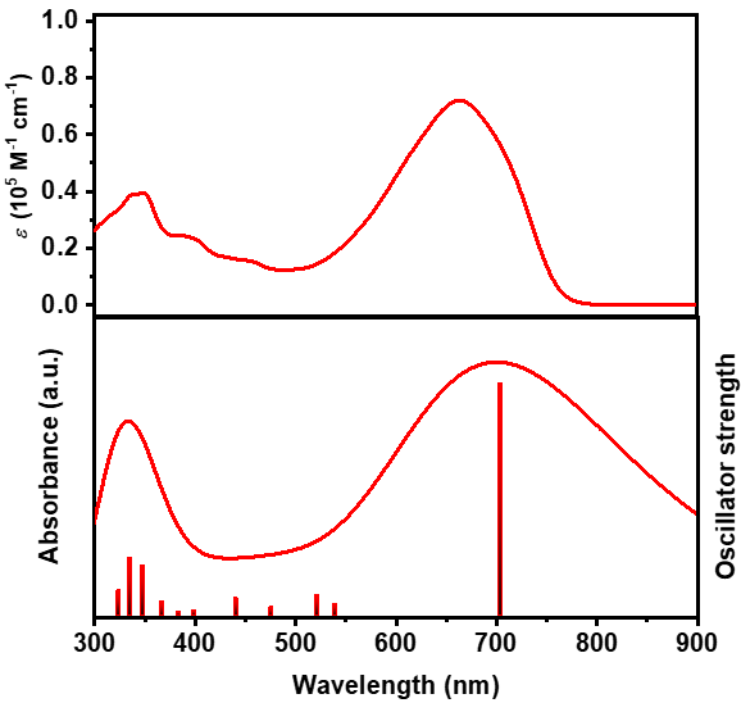

Figure S14. The experimental (top) and calculated (bottom) UV-Vis absorption spectra of APD-DPP. The major excitations (oscillator strength > 0.05) are shown in the bottom figure as vertical lines.

Table S6. Summary of the TD-DFT calculation results of APD-DPP.

Excited states	Energy (eV)	Wavelength (nm)	Oscillator strength	Major contributions
S1	1.7598	704.54	1.8512	HOMO→LUMO (99%)
S3	2.2954	540.14	0.0970	HOMO–1→LUMO+3 (2%) HOMO→LUMO+2 (85%) HOMO→LUMO+4 (4%)
S5	2.3769	521.61	0.1651	HOMO–2→LUMO (65%) HOMO–1→LUMO+1 (4%) HOMO→LUMO+2 (7%) HOMO→LUMO+4 (20%)
S7	2.6013	476.62	0.0689	HOMO–4→LUMO (4%) HOMO–2→LUMO (24%) HOMO–2→LUMO+2 (3%) HOMO–1→LUMO+1 (3%) HOMO–1→LUMO+3 (65%) HOMO→LUMO+4 (4%)
S10	2.8097	441.28	0.1396	HOMO–4→LUMO (59%)

				HOMO–3→LUMO+1 (8%) HOMO–2→LUMO+4 (2%) HOMO–1→LUMO+1 (16%) HOMO–1→LUMO+3 (4%) HOMO→LUMO+4 (3%)
S13	2.9224	424.25	0.0804	HOMO–4→LUMO (7%) HOMO–2→LUMO+2 (21%) HOMO–2→LUMO+4 (8%) HOMO–1→LUMO+3 (50%) HOMO→LUMO+4 (8%)

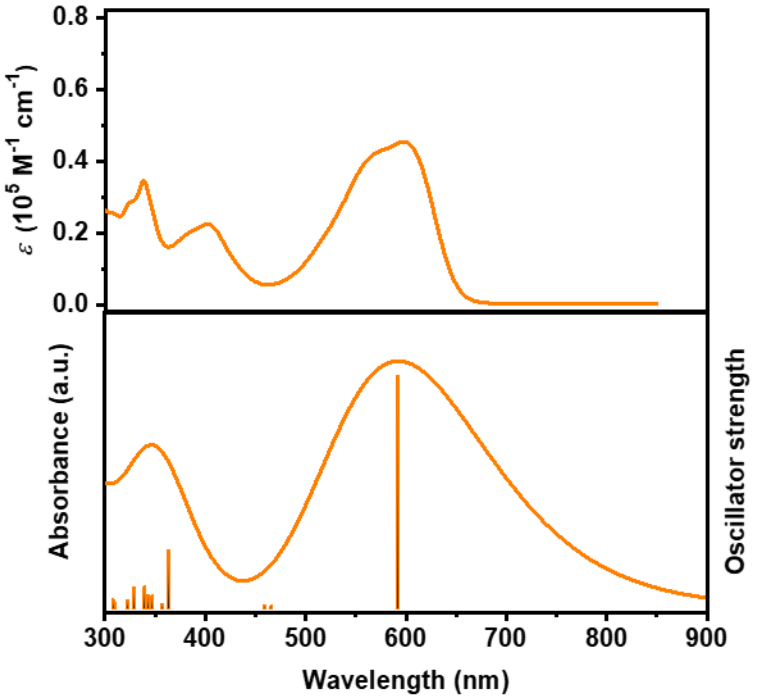

Figure S15. The experimental (top) and calculated (bottom) UV-Vis absorption spectra of 1Py-DPP. The major excitations (oscillator strength > 0.05) are shown in the bottom figure as vertical lines.

Table S7. Summary of the TD-DFT calculation results of 1Py-DPP.

Excited States	Energy (eV)	Wavelength (nm)	Oscillator Strength	Major Contributions
S1	2.0907	593.03	1.4371	HOMO→LUMO (99%)
S3	2.6565	466.71	0.0246	HOMO–2→LUMO (79%) HOMO→LUMO+2 (20%)
S4	2.6942	460.20	0.0255	HOMO–2→LUMO (38%) HOMO→LUMO+1 (61%)

S8	3.4060	364.02	0.3620	HOMO–6→LUMO (2%) HOMO–4→LUMO+1 (39%) HOMO–3→LUMO+1 (2%) HOMO–1→LUMO+3 (46%) HOMO→LUMO+4 (5%)
S10	3.4612	358.21	0.0344	HOMO–4→LUMO+1 (2%) HOMO–3→LUMO (48%) HOMO–2→LUMO+1 (29%) HOMO–1→LUMO+2 (5%) HOMO→LUMO+3 (6%) HOMO→LUMO+5 (5%)
S14	3.5637	347.90	0.0870	HOMO–4→LUMO (22%) HOMO–2→LUMO+2 (14%) HOMO–1→LUMO+1 (5%) HOMO→LUMO+4 (6%)
S15	3.6060	343.83	0.0928	HOMO–3→LUMO (20%) HOMO–2→LUMO+1 (4%) HOMO–1→LUMO+2 (42%) HOMO→LUMO+3 (7%) HOMO→LUMO+5 (19%)

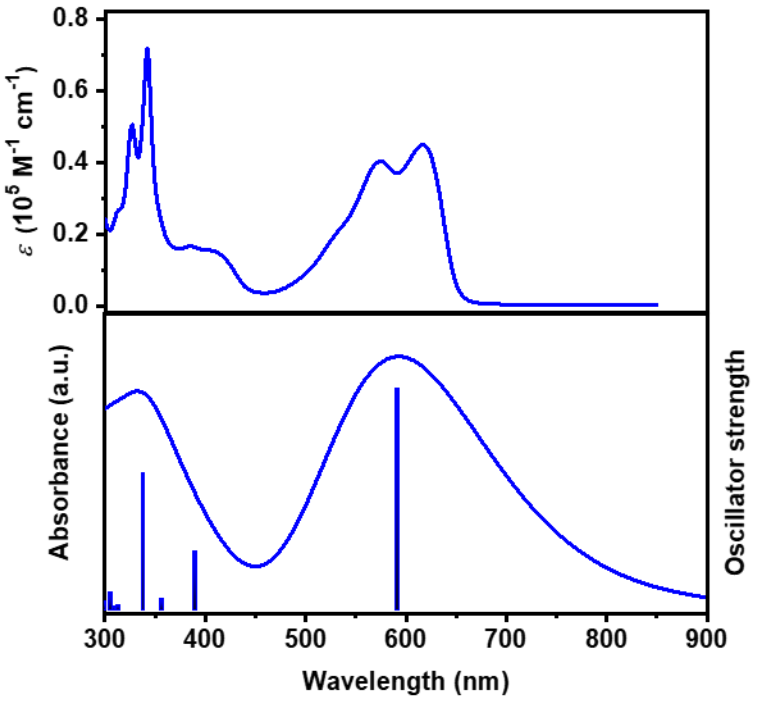

Figure S16. The experimental (top) and calculated (bottom) UV-Vis absorption spectra of 2Py-DPP. The major excitations (oscillator strength > 0.05) are shown in the bottom figure as vertical lines.

Table S8. Summary of the TD-DFT calculation results of 2Py-DPP.

Excited States	Energy (eV)	Wavelength (nm)	Oscillator Strength	Major Contributions
S1	2.0916	592.77	1.6429	HOMO→LUMO (98%)
S7	3.1805	389.83	0.4437	HOMO–4→LUMO (86%)
				HOMO→LUMO+4 (11%)
S10	3.4719	357.11	0.0859	HOMO–4→LUMO (10%)
				HOMO–2→LUMO+2 (5%)
				HOMO–1→LUMO+1 (5%)
				HOMO→LUMO+4 (76%)
S15	3.6608	338.68	1.0206	HOMO–4→LUMO+4 (2%)
				HOMO–3→LUMO+3 (4%)
				HOMO–2→LUMO+2 (36%)
				HOMO–1→LUMO+1 (36%)
				HOMO→LUMO+4 (10%)

Cartesian coordinates obtained in gas–phase DFT calculations

APD-DPP

Tag	Symbol	X	Y	Z
1	C	3.078580	–0.214915	–0.287541
2	C	0.610091	0.361836	–0.290886
3	C	–0.610097	–0.362037	–0.290961
4	C	–1.681394	0.534657	–0.290093
5	N	–1.129492	1.814516	–0.290185
6	C	0.303333	1.772185	–0.291673
7	C	1.681394	–0.534835	–0.289471
8	N	1.129507	–1.814709	–0.289347
9	C	–0.303313	–1.772385	–0.291219
10	C	–3.078585	0.214769	–0.288260
11	O	0.994144	2.783759	–0.294376
12	O	–0.994118	–2.783966	–0.293693
13	C	1.810446	–3.098501	–0.290663
14	C	–1.810457	3.098292	–0.293161
15	C	10.052006	–2.422571	–0.981669
16	C	11.353840	–2.014217	–0.684094
17	C	11.680389	–0.788217	–0.065006

18	C	10.595710	0.115449	0.284358
19	C	9.314506	–0.324842	–0.045260
20	C	9.001954	–1.573667	–0.660341
21	C	10.665620	1.410306	0.936256
22	C	9.457063	2.088293	1.193445
23	C	8.191660	1.602472	0.847863
24	C	8.103487	0.382625	0.197291
25	C	7.578067	–1.627893	–0.799939
26	C	7.016342	–0.457224	–0.298243
27	C	13.077823	–0.551605	0.161041
28	C	11.865637	2.078982	1.359952
29	C	13.723762	0.507079	0.729058
30	C	13.172596	1.701618	1.273779
31	C	–3.598431	–1.074483	–0.295975
32	C	–5.002007	–1.119391	–0.288806
33	C	–5.609977	0.124375	–0.277699
34	S	–4.397753	1.383463	–0.259832
35	C	3.598352	1.074359	–0.295022
36	C	5.001935	1.119351	–0.288020
37	C	5.609951	–0.124390	–0.277365
38	S	4.397830	–1.383549	–0.259677
39	C	–10.051904	2.423248	–0.980390
40	C	–11.353741	2.014869	–0.682895
41	C	–11.680341	0.788585	–0.064385
42	C	–10.595709	–0.115348	0.284438
43	C	–9.314495	0.324985	–0.045079
44	C	–9.001891	1.574088	–0.659580
45	C	–10.665687	–1.410515	0.935708
46	C	–9.457166	–2.088733	1.192456
47	C	–8.191749	–1.602857	0.846998
48	C	–8.103515	–0.382701	0.197015
49	C	–7.578046	1.628279	–0.799273
50	C	–7.016335	0.457303	–0.298237
51	C	–13.077770	0.551983	0.161672
52	C	–11.865720	–2.079291	1.359197
53	C	–13.723758	–0.506915	0.729238
54	C	–13.172653	–1.701769	1.273331
55	H	2.428725	–3.222362	–1.182425
56	H	2.426034	–3.226066	0.602444
57	H	1.029774	–3.858666	–0.293272
58	H	–1.029813	3.858479	–0.296779

59	H	–2.428780	3.220915	–1.185062
60	H	–2.426014	3.227058	0.599800
61	H	9.882872	–3.386224	–1.450327
62	H	12.173690	–2.677215	–0.937176
63	H	9.519542	3.047270	1.695509
64	H	7.314136	2.183083	1.105564
65	H	7.026960	–2.438519	–1.257094
66	H	13.718944	–1.358356	–0.183066
67	H	11.687425	3.044828	1.824098
68	H	14.805976	0.431987	0.776077
69	H	13.896019	2.404559	1.675988
70	H	–2.958561	–1.948405	–0.316106
71	H	–5.561647	–2.042752	–0.336411
72	H	2.958431	1.948250	–0.314961
73	H	5.561530	2.042749	–0.335460
74	H	–9.882710	3.387121	–1.448575
75	H	–12.173562	2.678061	–0.935564
76	H	–9.519673	–3.047950	1.694058
77	H	–7.314277	–2.183709	1.104332
78	H	–7.026920	2.439106	–1.256053
79	H	–13.718852	1.358959	–0.181982
80	H	–11.687542	–3.045374	1.822862
81	H	–14.805960	–0.431743	0.776393
82	H	–13.896105	–2.404836	1.675267

1Py-DPP

Tag	Symbol	X	Y	Z
1	C	–3.058950	–0.422189	–0.642308
2	C	–0.523932	–0.479746	–0.653994
3	C	0.523866	0.479188	–0.654177
4	C	1.753379	–0.179461	–0.647544
5	N	1.477112	–1.544712	–0.647142
6	C	0.064775	–1.797350	–0.650673
7	C	–1.753441	0.178912	–0.647770
8	N	–1.477166	1.544161	–0.647983
9	C	–0.064837	1.796798	–0.651561
10	C	3.058877	0.421674	–0.642298
11	O	–0.403370	–2.928658	–0.652716

12	O	0.403319	2.928101	–0.654087
13	C	–2.406756	2.661394	–0.661643
14	C	2.406683	–2.661969	–0.659963
15	C	–6.988195	–1.035956	–0.665558
16	C	3.303881	1.787111	–0.650828
17	C	4.673982	2.113934	–0.633431
18	C	5.516994	1.023837	–0.597656
19	S	4.586783	–0.454743	–0.612965
20	C	–3.303961	–1.787626	–0.650250
21	C	–4.674060	–2.114448	–0.632644
22	C	–5.517082	–1.024358	–0.597224
23	S	–4.586856	0.454255	–0.613155
24	C	6.988113	1.035497	–0.666059
25	C	7.825214	0.328835	0.236737
26	C	9.243513	0.379382	0.054128
27	C	9.808001	1.149513	–1.005399
28	C	8.949686	1.862606	–1.853163
29	C	7.575942	1.801260	–1.685759
30	C	10.108936	–0.334716	0.937571
31	C	9.567560	–1.086741	2.020275
32	C	10.434664	–1.784866	2.874173
33	C	11.810724	–1.748760	2.673413
34	C	12.351015	–1.012797	1.622939
35	C	11.522969	–0.296990	0.745731
36	C	12.052244	0.478340	–0.339738
37	C	11.232662	1.171483	–1.172752
38	C	7.320014	–0.409609	1.361936
39	C	8.146904	–1.082780	2.205480
40	C	–7.825197	–0.328718	0.236878
41	C	–9.243505	–0.379232	0.054357
42	C	–9.808113	–1.149892	–1.004721
43	C	–8.949902	–1.863552	–1.852112
44	C	–7.576144	–1.802247	–1.684793
45	C	–10.108831	0.335423	0.937448
46	C	–9.567342	1.087983	2.019720
47	C	–10.434342	1.786635	2.873293
48	C	–11.810416	1.750532	2.672622
49	C	–12.350818	1.014052	1.622565
50	C	–11.522876	0.297711	0.745698
51	C	–7.319881	0.410281	1.361664
52	C	–8.146676	1.083991	2.204871

53	C	–12.052272	–0.478155	–0.339334
54	C	–11.232786	–1.171818	–1.172008
55	H	–3.042836	2.641190	–1.549176
56	H	–3.030089	2.675701	0.235047
57	H	–1.798432	3.565154	–0.682462
58	H	1.798336	–3.565732	–0.680002
59	H	3.042699	–2.642521	–1.547561
60	H	3.030082	–2.675543	0.236690
61	H	2.500740	2.514054	–0.660044
62	H	5.044244	3.130809	–0.625854
63	H	–2.500837	–2.514591	–0.659202
64	H	–5.044270	–3.131339	–0.624636
65	H	9.368912	2.453033	–2.660799
66	H	6.929174	2.330659	–2.375322
67	H	10.019081	–2.355028	3.698181
68	H	12.467170	–2.294752	3.341538
69	H	13.425294	–0.985590	1.474525
70	H	13.127688	0.503578	–0.480611
71	H	11.645396	1.758516	–1.986421
72	H	6.254893	–0.414706	1.548394
73	H	7.734411	–1.625555	3.049615
74	H	–9.369209	–2.454387	–2.659407
75	H	–6.929477	–2.332106	–2.374096
76	H	–10.018670	2.357199	3.696977
77	H	–12.466787	2.296929	3.340490
78	H	–13.425106	0.986851	1.474221
79	H	–6.254753	0.415367	1.548087
80	H	–7.734105	1.627189	3.048695
81	H	–13.127724	–0.503371	–0.480146
82	H	–11.645596	–1.759246	–1.985353

2Py-DPP

Tag	Symbol	X	Y	Z
1	C	0.565505	–0.428468	–0.216201
2	C	–0.565502	0.428947	–0.216201
3	C	–1.728981	–0.340175	–0.202537
4	N	–1.328409	–1.673447	–0.201738
5	C	0.101439	–1.795811	–0.211149
6	C	1.728978	0.340631	–0.201907
7	N	1.328410	1.673909	–0.200647

8	C	–0.101434	1.796288	–0.210507
9	O	0.669045	–2.878764	–0.217767
10	O	–0.669024	2.879251	–0.216859
11	C	3.082006	–0.139945	–0.182276
12	C	–3.082031	0.140336	–0.182958
13	C	3.449201	–1.478009	–0.204618
14	C	–3.449339	1.478368	–0.205239
15	C	–4.839856	1.681954	–0.162453
16	C	–5.579355	0.518750	–0.106216
17	S	–4.522620	–0.868864	–0.096036
18	C	4.839703	–1.681727	–0.161964
19	C	5.579295	–0.518581	–0.105771
20	S	4.522720	0.869128	–0.095751
21	C	7.035144	–0.364559	–0.042595
22	C	–7.035176	0.364600	–0.042933
23	C	–2.147890	–2.872922	–0.210527
24	C	2.147882	2.873382	–0.208395
25	C	7.817634	–1.372408	0.540853
26	C	9.209156	–1.265404	0.616975
27	C	9.848784	–0.101754	0.097861
28	C	9.060323	0.927871	–0.493408
29	C	7.671784	0.775051	–0.554869
30	C	–7.817754	1.372606	0.540132
31	C	–9.209258	1.265477	0.616394
32	C	–9.848790	0.101529	0.097830
33	C	–9.060248	–0.928256	–0.493051
34	C	–7.671734	–0.775300	–0.554676
35	C	–11.263154	–0.032861	0.173432
36	C	–12.046958	0.997818	0.771303
37	C	–13.438338	0.841676	0.835550
38	C	–14.050339	–0.299248	0.325085
39	C	–13.292571	–1.309013	–0.260140
40	C	–11.897870	–1.198858	–0.347616
41	C	–10.025215	2.286583	1.215182
42	C	–11.375274	2.158328	1.287569
43	C	–11.078521	–2.217458	–0.943460
44	C	–9.728147	–2.089629	–1.013762
45	C	11.263172	0.032498	0.173292
46	C	12.046898	–0.998013	0.771551
47	C	13.438304	–0.842014	0.835613
48	C	14.050403	0.298609	0.324591

49	C	13.292710	1.308209	–0.261012
50	C	11.897988	1.198188	–0.348321
51	C	10.025037	–2.286345	1.216148
52	C	11.375116	–2.158215	1.288380
53	C	11.078717	2.216629	–0.944542
54	C	9.728321	2.088934	–1.014680
55	H	2.714303	–2.272237	–0.255461
56	H	–2.714522	2.272669	–0.256035
57	H	–5.295530	2.662249	–0.201197
58	H	5.295304	–2.662056	–0.200680
59	H	–1.453977	–3.712669	–0.233445
60	H	–2.763125	–2.946723	0.689024
61	H	–2.787356	–2.914897	–1.095010
62	H	2.787262	2.916228	–1.092905
63	H	1.453969	3.713152	–0.230482
64	H	2.763201	2.946325	0.691163
65	H	7.335540	–2.243494	0.969267
66	H	7.082699	1.551169	–1.031115
67	H	–7.335746	2.243928	0.968164
68	H	–7.082604	–1.551568	–1.030624
69	H	–14.038109	1.623132	1.289829
70	H	–15.127979	–0.402310	0.383910
71	H	–13.779260	–2.194442	–0.655030
72	H	–9.536288	3.170033	1.611862
73	H	–11.974983	2.939747	1.742426
74	H	–11.565416	–3.101974	–1.340584
75	H	–9.126538	–2.870402	–1.466955
76	H	14.038017	–1.623343	1.290188
77	H	15.128061	0.401562	0.383276
78	H	13.779475	2.193405	–0.656333
79	H	9.536035	–3.169566	1.613245
80	H	11.974768	–2.939504	1.743537
81	H	11.565689	3.100911	–1.342092
82	H	9.126771	2.869582	–1.468165

8. References

1. L. Fu, P. Liu, R. Xue, X.-Y. Tang, J. Cao, Z.-F. Yao, Y. Liu, S. Yan and X.-Y. Wang, *Angew. Chem. Int. Ed.*, 2023, **62**, e202306509.
2. H. Li, F. Liu, X. Wang, C. Gu, P. Wang and H. Fu, *Macromolecules*, 2013, **46**, 9211.
3. O. P. Lee, A. T. Yiu, P. M. Beaujuge, C. H. Woo, T. W. Holcombe, J. E. Millstone, J. D. Douglas, M. S. Chen, and J. M. J. Fréchet, *Adv. Mater.*, 2011, **23**, 5359.
4. D. Liu, Z. He, Y. Su, Y. Diao, S. C. B. Mannsfeld, Z. Bao, J. Xu and Q. Miao, *Adv. Mater.*, 2014, **26**, 7190.
5. M. Li, C. An, T. Marszalek, X. Guo, Y.-Z. Long, H. Yin, C. Gu, M. Baumgarten, W. Pisula and K. Müllen, *Chem. Mater.*, 2015, **27**, 2218.
6. M. Zhu, S. Lv, Q. Wang, G. Zhang, H. Lu and L. Qiu, *Nanoscale*, 2016, **8**, 7738.
7. Y. He, J. T. E. Quinn, D. Hou, J. H. L. Ngai and Y. Li, *J. Mater. Chem. C*, 2017, **5**, 12163.
8. M. J. Kim, S. Choi, M. Lee, H. Heo, Y. Lee, J. H. Cho and B. Kim, *ACS Appl. Mater. Interfaces*, 2017, **9**, 19011.
9. F. Li, Y. Chen, C. Ma, U. Buttner, K. Leo and T. Wu, *Adv. Electron. Mater.*, 2017, **3**, 1600430.
10. S. Lee, C. Lee, H. Kim and Y. Kim, *J. Mater. Chem. C*, 2020, **8**, 15778.
11. C. Xiao, C. Li, F. Liu, L. Zhang and W. Li, *J. Mater. Chem. C*, 2020, **8**, 5370.
12. S. Kim, D. Lee, J. Lee, Y. Cho, S.-H. Kang, W. Choi, J. H. Oh and C. Yang, *Chem. Mater.*, 2021, **33**, 7499.
13. J. Park, C. Lee, T. Kim, H. Kim and Y. Kim, *Adv. Electron. Mater.*, 2021, **7**, 2000932.
14. H. Son, T. Kim, C. Lee, H. Kim and Y. Kim, *J. Mater. Chem. C*, 2022, **10**, 3951.
15. Y. Cho, T. Kim, W. Lee, H. Kim and Y. Kim, *J. Mater. Chem. C*, 2023, **11**, 2970.
16. Gaussian 09, Revision D.01, M. J. Frisch, G. W. Trucks, H. B. Schlegel, G. E. Scuseria, M. A. Robb, J. R. Cheeseman, G. Scalmani, V. Barone, B. Mennucci, G. A. Petersson, H. Nakatsuji, M. Caricato, X. Li, H. P. Hratchian, A. F. Izmaylov, J. Bloino, G. Zheng, J. L. Sonnenberg, M. Hada, M. Ehara, K. Toyota, R. Fukuda, J. Hasegawa, M. Ishida, T. Nakajima, Y. Honda, O. Kitao, H. Nakai, T. Vreven, J. A. Montgomery, Jr., J. E. Peralta, F. Ogliaro, M. Bearpark, J. J. Heyd, E. Brothers, K. N. Kudin, V. N. Staroverov, T. Keith, R. Kobayashi, J. Normand, K. Raghavachari, A. Rendell, J. C. Burant, S. S. Iyengar, J. Tomasi, M. Cossi, N. Rega, J. M. Millam, M. Klene, J. E. Knox, J. B. Cross, V. Bakken, C. Adamo, J. Jaramillo, R. Gomperts, R. E. Stratmann, O. Yazyev, A. J. Austin, R. Cammi, C. Pomelli, J. W. Ochterski, R. L. Martin, K. Morokuma, V. G. Zakrzewski, G. A. Voth, P. Salvador, J. J. Dannenberg, S. Dapprich, A. D. Daniels, O. Farkas, J. B. Foresman, J. V. Ortiz, J. Cioslowski, and D. J. Fox, Gaussian, Inc., Wallingford CT, 2013.
17. (a) A. D. Becke, *J. Chem. Phys.* 1993, **98**, 5648. (b) C. Lee, W. Yang, R. G. Parr, *Phys. Rev. B* 1988, **37**, 785. (c) T. Yanai, D. Tew, N. Handy, *Chem. Phys. Lett.* 2004, **393**, 51. (d) R. Ditchfield, W. J. Hehre, J. A. Pople, *Chem. Phys.* 1971, **54**, 724. (e) W. J. Hehre, R. Ditchfield, J. A. Pople, *Chem. Phys.* 1972, **56**, 2257. (f) P. C. Hariharan, J. A. Pople, *Theor. Chim. Acta.* 1973, **28**, 213.

9. NMR Spectra

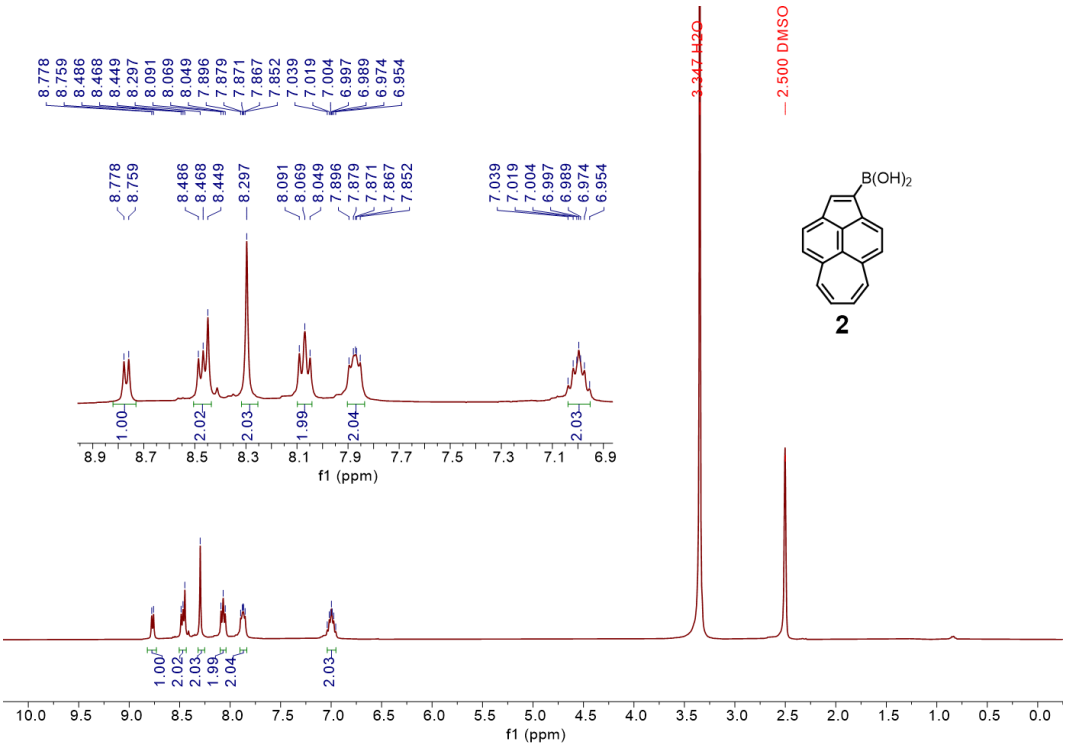

Figure S17. ^{1}H NMR spectrum of compound **2** (400 MHz, DMSO-d_6, 298 K).

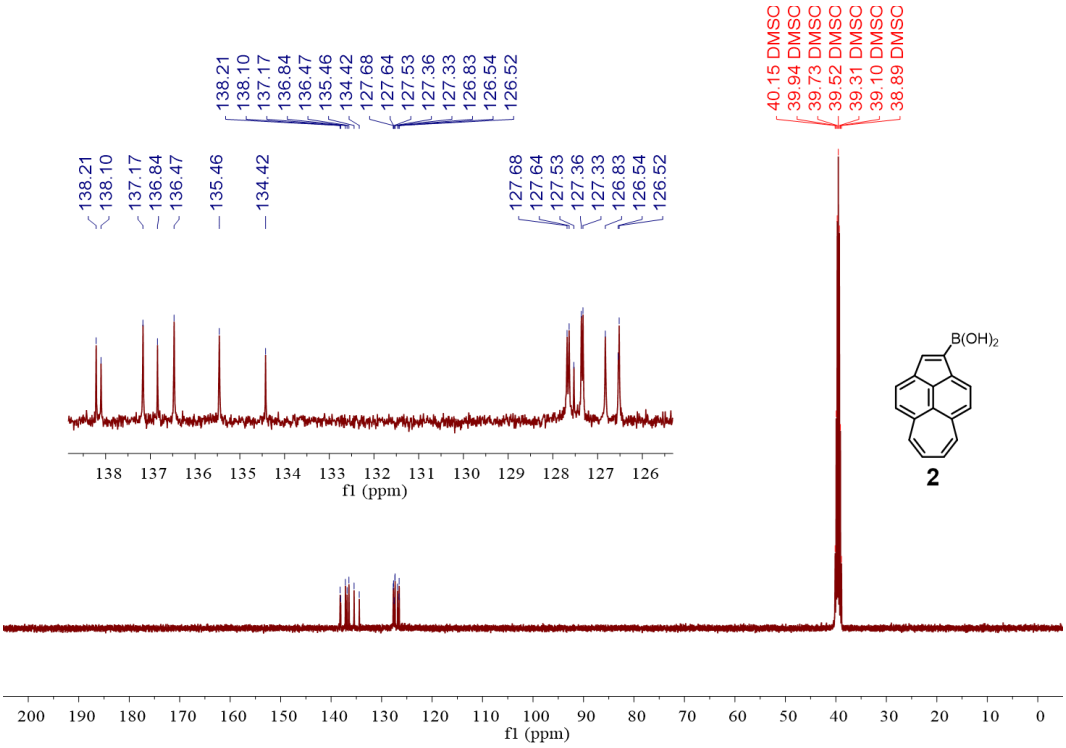

Figure S18. ^{13}C NMR spectrum of compound **2** (101 MHz, DMSO-d_6, 298 K).

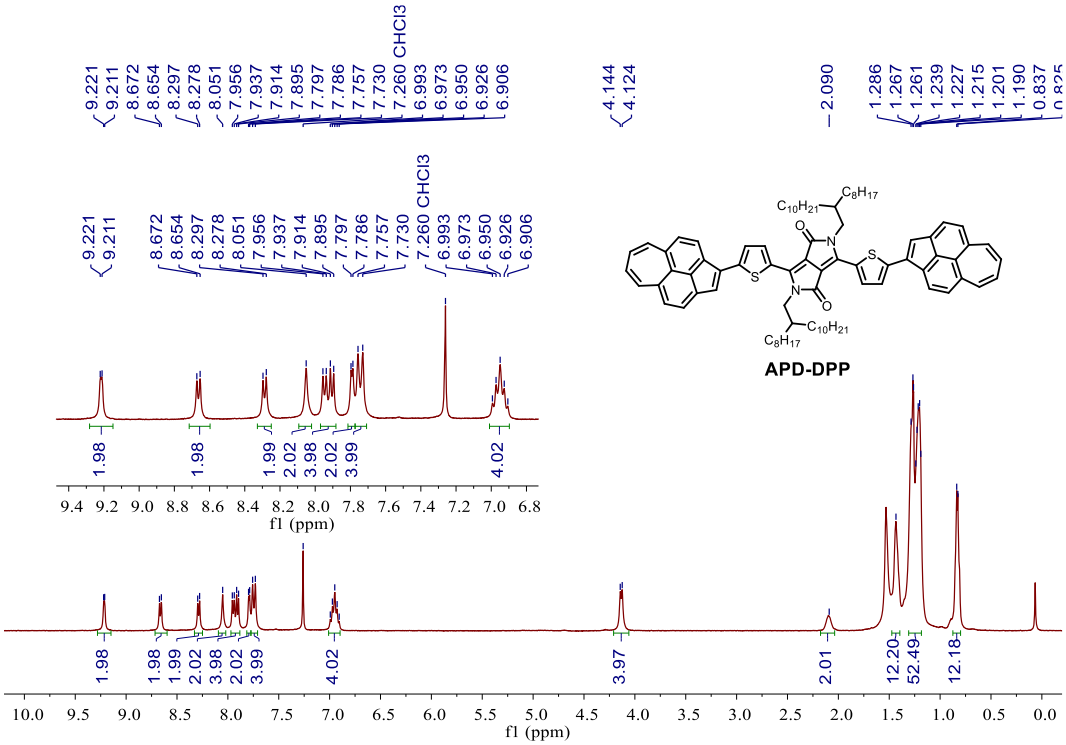

Figure S19. ^{1}H NMR spectrum of APD-DPP (400 MHz, $CDCl_3$, 298 K).

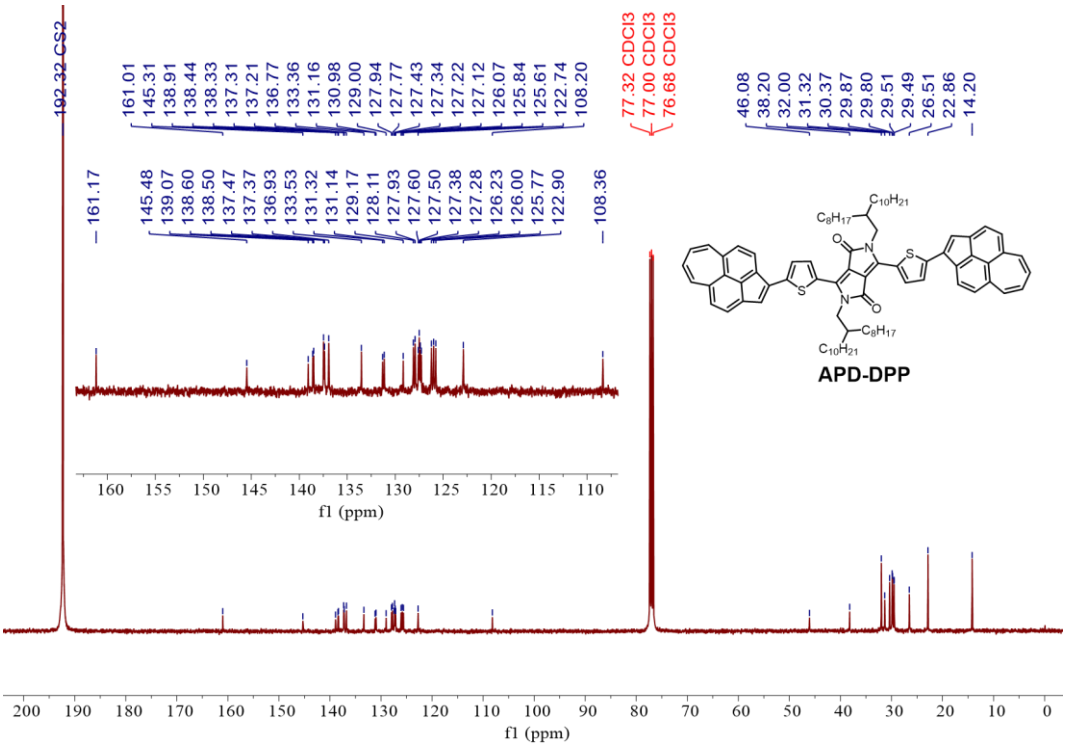

Figure S20. ^{13}C NMR spectrum of APD-DPP (101 MHz, CS_2/$CDCl_3$, 298 K).

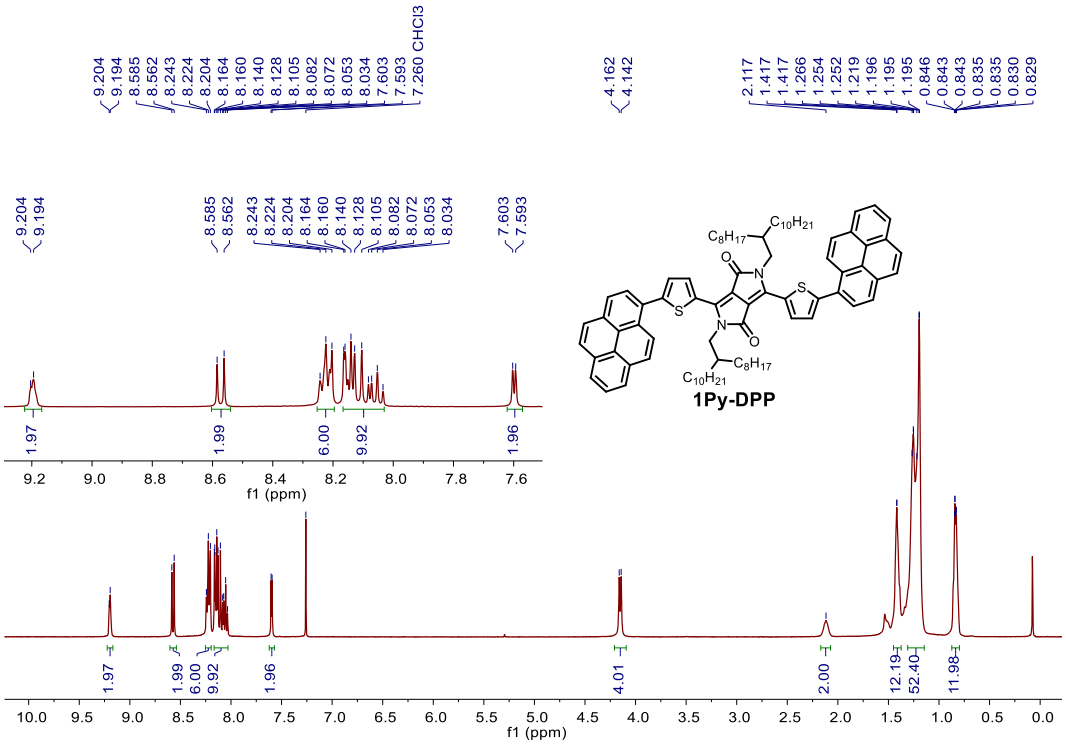

Figure S21. ^{1}H NMR spectrum of 1Py-DPP (400 MHz, $CDCl_3$, 298 K).

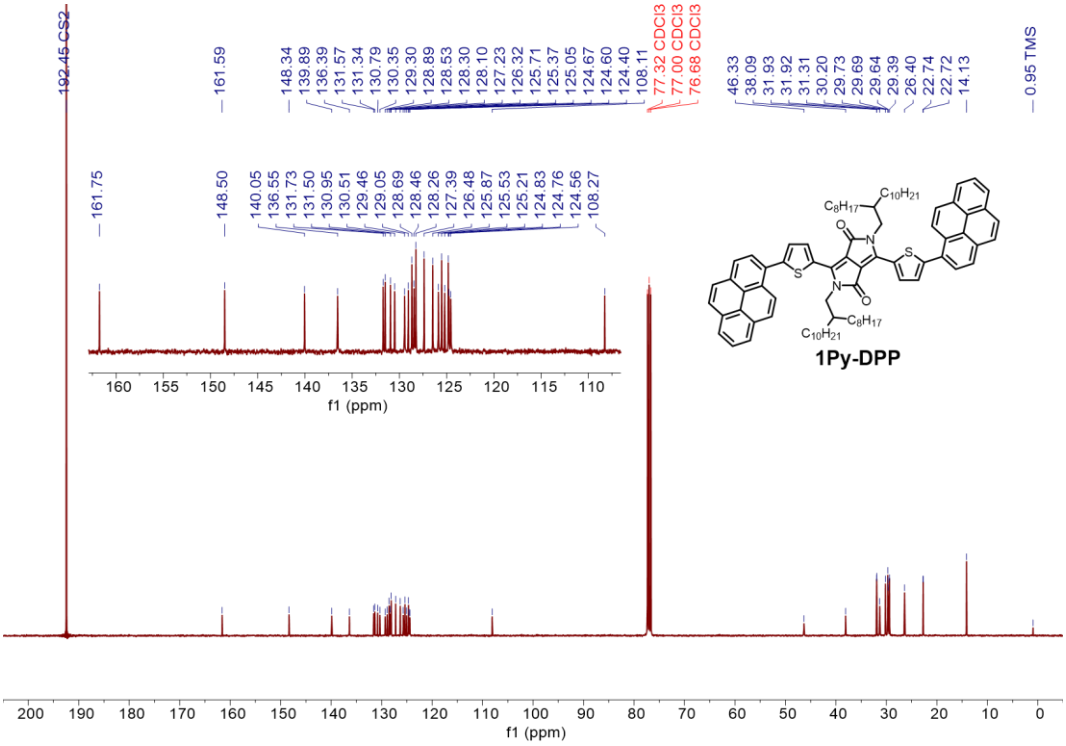

Figure S22. ^{13}C NMR spectrum of 1Py-DPP (101 MHz, CS_2/$CDCl_3$, 298 K).

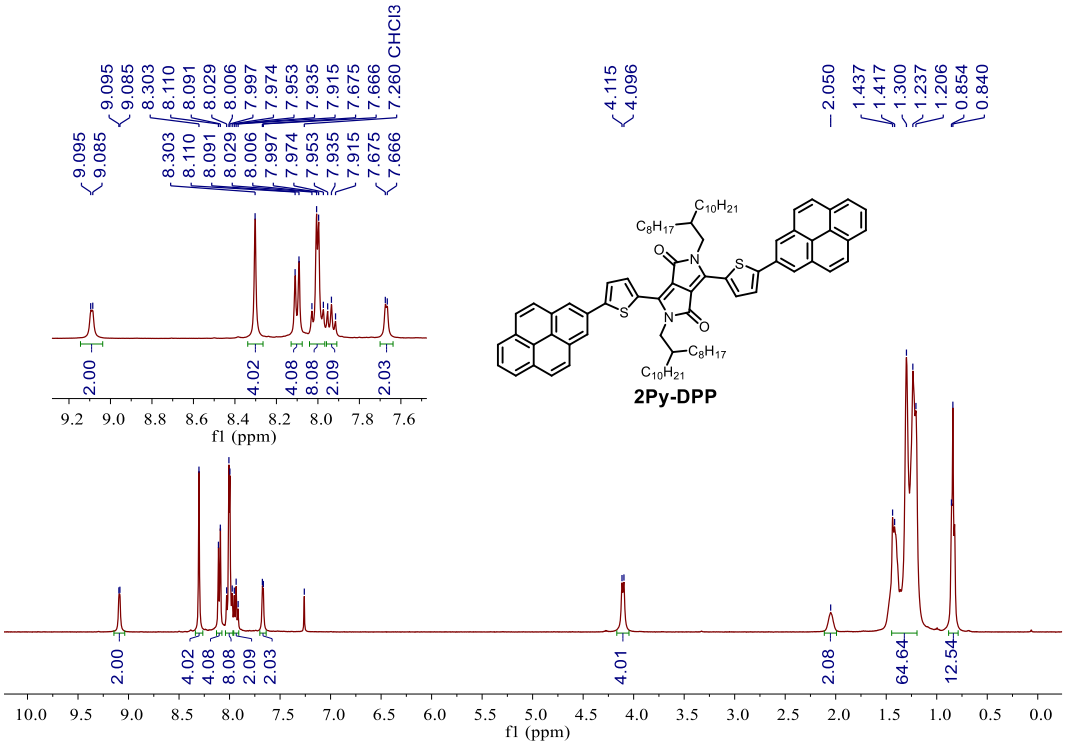

Figure S23. ^{1}H NMR spectrum of 2Py-DPP (400 MHz, $CDCl_3$, 298 K).

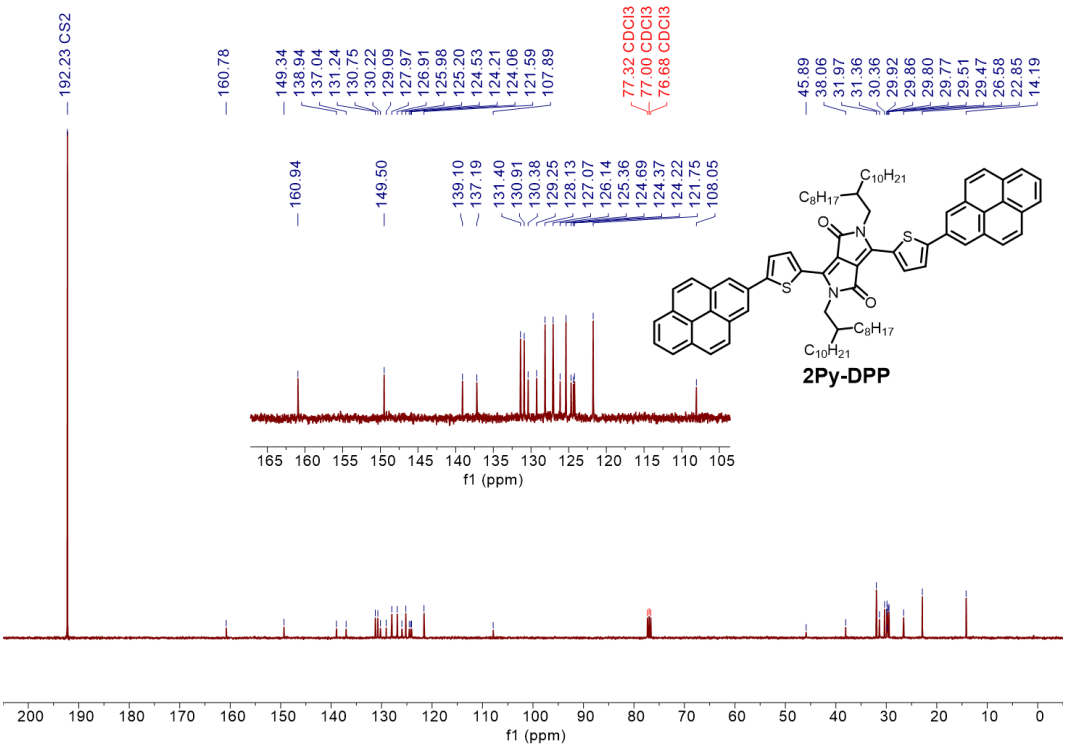

Figure S24. ^{13}C NMR spectrum of 2Py-DPP (101 MHz, CS_2/$CDCl_3$, 298 K).